The Astrophysical Journal, 640:435–440, 2006 March 20

X-RAY AND INFRARED ENHANCEMENT OF ANOMALOUS X-RAY PULSAR 1E 2259+586

Ü. Ertan, E. Göğüş, and M. A. Alpar
Faculty of Engineering and Natural Sciences, Sabancı University, Orhanlı–Tuzla 34956 İstanbul, Turkey
Received 2005 January 6; accepted 2005 November 28

ABSTRACT

The long-term (∼1.5 yr) X-ray enhancement and the accompanying infrared enhancement light curves of the anomalous X-ray pulsar 1E 2259+586 following the major bursting epoch can be accounted for by the relaxation of a fallback disk that has been pushed back by a gamma-ray flare. The required burst energy estimated from the results of our model fits is low enough for such a burst to have remained below the detection limits. We find that an irradiated disk model with a low irradiation efficiency is in good agreement with both X-ray and infrared data. Nonirradiated disk models also give a good fit to the X-ray light curve, but are not consistent with the infrared data for the first week of the enhancement.

Subject headings: accretion, accretion disks — pulsars: individual (1E 2259+586) — stars: neutron — X-rays: bursts

1. INTRODUCTION

Anomalous X-ray pulsars (AXPs) and soft gamma-ray repeaters (SGRs) are neutron stars that are characterized by persistent X-ray luminosities ($L \sim 10^{34}-10^{36}$ ergs s^{-1}) well above their rotation powers (see Mereghetti et al. 2002; Hurley 2000 for reviews of AXPs and SGRs, respectively). Another remarkable property of these sources is the clustering of their spin periods to a very narrow range ($P \sim 5-12$ s). There is no observational evidence for a binary nature in these systems. They exhibit short ($\lesssim$1 s), super-Eddington ($\lesssim 10^{42}$ ergs s^{-1}) bursts. Burst repetition timescales vary from seconds to years. In about three decades of observations of these sources, three giant flares were observed from the SGRs 0526−66 (Mazets et al. 1979), 1900+14 (Hurley et al. 1999), and 1806−20 (Palmer et al. 2005). These giant flares are characterized by an initial hard spike with a peak luminosity $\geq 10^{44}$ ergs s^{-1} that lasts a fraction of a second. The hard spike is followed by an oscillating tail that decays in a few minutes. Assuming isotropic emission, the fluence of the entire giant flare is $\gtrsim 10^{44}$ ergs (Hurley et al. 1999; Feroci et al. 2001; Mazets et al. 1999). Following the 1998 August 27 giant burst of SGR 1900+14, the persistent X-ray flux increased by a factor of ∼700 to a peak luminosity of $\sim 10^{38}$ ergs s^{-1}. The subsequent decay is a power law with index ∼0.7 (Woods et al. 2001). The three other, less luminous X-ray enhancements of SGR 1900+14 were also preceded by gamma-ray flares. An X-ray enhancement was also observed from AXP 1E 2259+586. Although no strong burst preceding the enhancement was reported, it is possible that such a burst could have been missed (Woods et al. 2004). Out of six known AXPs including 1E 2259+586, five sources were detected in the IR band (Hulleman et al. 2001, 2004; Israel et al. 2002, 2003, 2004; Wang & Chakrabarty 2002; Kaspi et al. 2003). One of them, 4U 0142+61, was also observed in the optical (R) band (Hulleman et al. 2000; Dhillon et al. 2005). The optical flux from AXP 4U 0142+61 has a pulsed component with a pulsed fraction (∼0.27) much higher than the observed pulsed fraction (∼0.05) in X-rays (Kern & Martin 2002). Observations of the transient AXP XTE J1810−197 separated by a few months showed a correlated decrease (by a factor of ∼2) in X-ray and IR luminosities (Rea et al. 2004; Israel et al. 2004). IR radiation from this source was proposed to be radiated from a passive disk irradiated by the X-rays from the neutron star (Rea et al. 2004). In this model, the source of the X-rays is assumed to have a magnetic origin, as proposed by the magnetar models, rather than accretion onto the neutron star. The X-ray enhancement of AXP 1E 2259+586 was also accompanied by an enhancement in the IR luminosity (Kaspi et al. 2003). Long-term (∼1.5 yr) IR and X-ray flux evolutions of this source exhibited a correlated decay behavior (Tam et al. 2004).

The magnetar model (Duncan & Thompson 1992; Thompson & Duncan 1995) can explain the energies and the super-Eddington luminosities of the normal and the giant bursts of these sources. In these models, the source of the bursts is the huge magnetic energy release from inside the neutron stars. The persistent X-ray emission was suggested to originate from the magnetic field decay (Thompson & Duncan 1996). The spin-down torque is provided by the magnetic dipole radiation. Magnetar models have no detailed predictions for the observed optical and infrared (IR) emission from AXPs and cannot explain the period clustering of AXPs and SGRs without assuming special conditions (Colpi et al. 2000).

Fallback disk models (Chatterjee et al. 2000; Alpar 2001; Marsden et al. 2001) explain the period clustering of these sources using conventional dipole magnetic fields of young neutron stars with $B_* \sim 10^{12}-10^{13}$ G on the surface of the neutron star within the timescales of the ages of their associated supernova remnants (Chatterjee & Hernquist 2000; Ekşi & Alpar 2003). In fallback disk models, the source of the X-ray luminosity is the accretion onto the neutron star from the accretion disk. In earlier work (Ertan & Alpar 2003), we showed, by means of numerical fits to data, that the X-ray enhancement of the SGR 1900+14 following its giant flare can be reproduced by the relaxation of the inner disk subsequent to an initial push back caused by the flare. We estimated that part of the pushed back inner disk piles up and remains bound, creating the postburst initial conditions of the disk, while the remaining part escapes from the system. The estimated energetics and the amount of escaping ejecta can account for the observed radio enhancement accompanying the X-ray enhancement of the SGR 1900+14 (Ertan & Cheng 2004b). An important limitation for the models is the observed optical and IR emission from the AXPs. It was shown that the observed pulsed component of AXP 4U 0142+61 can be explained by both the magnetar outer gap models and the disk-star dynamo models (Ertan & Cheng 2004a). Furthermore,

unpulsed optical/IR emission from the AXP 4U 0142+61 is in agreement with the expectations of a standard thin-disk model (Ertan & Cheng 2004a). In the disk models, the inner radius of the disk is consistent with a dipole component of the magnetic field with a strength of $\sim 10^{12}$ G on the stellar surface. The origin of energetic bursts requires magnetar-strength surface fields. It could be the case that the burst involves surface magnetar fields in the higher multipole components, while a disk standing at an inner radius set by a 10^{12} G surface dipole field defines the rotation period of the star in a near-equilibrium state. It seems that such a hybrid model can explain almost all the observational behaviors of the AXPs and SGRs.

The enhancement energetics of the SGR 1900+14 and the AXP 1E 2259+586 are different. While the SGR 1900+14 was observed only in X-rays, we now have contemporaneous X-ray and IR enhancement data for the AXP 1E 2259+586. In this work, our aim is to answer the following: (1) Is it possible to explain the X-ray enhancement of the AXP 1E 2259+586 by using a pushed back disk model similar to that applied to the SGR 1900+14? (2) Is this model capable of reproducing both the X-ray and the IR data of the AXP 1E 2259+586? In answering these questions, we test both irradiated and nonirradiated disk models. We estimate the required burst energy to build up postburst initial inner disk conditions for the enhanced radiation and check whether such a burst could have remained below detection limits.

The 2–10 keV X-ray flux data of AXP 1E 2259+586 were taken from Woods et al. (2004). They monitored the source with the *Rossi X-ray Timing Explorer* (*RXTE*) Proportional Counter Array and determined the pulsed X-ray intensity of the source over a large time baseline. Using pointed *XMM-Newton* observations, they derived a conversion factor between the pulsed intensity and unabsorbed flux for this source. A detailed description of this conversion is given in Woods et al. (2004).

The infrared measurements of 1E 2259+586 were obtained from Kaspi et al. (2003), Israel et al. (2003), and Tam et al. (2004). The first two observations were made with the Near-Infrared Imager (NIRI) at the Gemini North telescope at about 3 and 10 days after the onset of the bursting activity. In these pointings, the K_s magnitudes of the source were found to be 20.36 ± 0.15 and 21.14 ± 0.21, respectively (Kaspi et al. 2003). The third infrared measurement, carried out with the Canada-France-Hawaii Telescope, gave a K' magnitude of 21.31 ± 0.24 (Israel et al. 2003). The last two observations were also made with NIRI and resulted in K_s magnitudes of 21.66 ± 0.11 and 21.54 ± 0.05, respectively. We converted these magnitudes into physical flux units using the method described in Tam et al. (2004). Details of the irradiated and nonirradiated disk models are given in § 2. The results are discussed in § 3. We summarize our conclusions in § 4.

2. THE NUMERICAL MODEL

All four observed X-ray enhancements of the SGR 1900+14 were preceded by strong gamma-ray flares. No gamma-ray burst was reported before the onset of the X-ray enhancement of the AXP 1E 2259+586. It is possible that such a burst could have remained below the detection limits. We assume that the X-ray enhancement of the AXP 1E 2259+586 was preceded by a missed gamma-ray burst. We discuss the burst fluence required to build up the postburst initial disk conditions and the observational limits in § 3. In earlier work (Ertan & Alpar 2003), we showed that the X-ray enhancement evolution of the SGR 1900+14 following the August 27 giant flare can be accounted for by the relaxation of inner disk matter that has been pushed back by the flare. We apply the same model to AXP 1E 2259+586, assuming that the physical mechanism giving rise to the X-ray enhancement is the same. Our aim is to explain the observed X-ray enhancement together with the accompanying IR enhancement data. In our model, the source of the X-rays is accretion onto the neutron star, while the IR emission originates from the accretion disk. We investigate the IR emission for both irradiated and nonirradiated disk models.

In our numerical model, we take the model functional form of the postburst initial mass distribution to be the same as that applied to SGR 1900+14 (Ertan & Alpar 2003). The part of the inner disk matter pushed back by the flare energy that remains bound to the system is represented by a Gaussian, $\Sigma(R, t = 0) = \Sigma_{\max} \exp\{-[(R - R_0)/\Delta R]^2\}$, centered at the radius R_0. Added to this Gaussian is a surface density profile in the form $\Sigma = \Sigma_0 (R_0/R)^p$, which represents the extended outer disk. The inner disk radius $R_{\rm in}$, where the inflowing disk matter is stopped by the magnetic pressure, is kept constant. We numerically solve the disk diffusion equation for the surface density, as described in detail in Ertan & Alpar (2003). We use the α prescription of the kinematic viscosity $\nu = \alpha c_s h$ (Shakura & Sunyaev 1973), where $c_s = kT_c/\mu m_p$ is the local sound speed, T_c is the local disk midplane temperature, $h = c_s/\Omega_{\rm K}$ is the pressure scale height of the disk, and $\Omega_{\rm K}$ is the local Keplerian angular velocity of the disk. The viscosity parameter $\alpha = 0.08$ and the outer disk radius $R_{\rm out} = 10^{12}$ cm are kept constant throughout the calculations. The chosen $R_{\rm out}$ is large enough that it does not affect the results.

2.1. *X-Ray Emission from the Neutron Star Surface*

For a thin disk, the total disk luminosity is $L_{\rm disk} = GM\dot{M}_{\rm in}/2R_{\rm in}$, and most of this emission comes from the inner disk. Here, $\dot{M}_{\rm in}$ is the mass inflow rate arriving at the inner disk radius $R_{\rm in}$, and M is the mass of the neutron star, which we take to be 1.4 $M_\odot$. The accretion luminosity from the neutron star surface, $L_* = GM\dot{M}_*/R_*$, determines the observed luminosity in the X-ray band. Assuming that most of the X-ray flux from the source is emitted in the observation band (2–10 keV), we take the observed X-ray luminosity to represent the total luminosity L_* of the neutron star. The evolution of the X-ray luminosity depends on both $\dot{M}_{\rm in}(t)$ and its fraction accreted onto the neutron star $f = \dot{M}_*/\dot{M}_{\rm in}$, where $\dot{M}_*$ is the mass accretion rate onto the star. The X-ray luminosity can be written as $L_* = 2f(R_{\rm in}/R_*)L_{\rm disk}$. We compare the energy flux $F_* \sim L_*/(4\pi d^2)$ with the X-ray data for the model fits. We take the distance of the source $d = 5$ kpc (Hulleman et al. 2000).

2.2. *Infrared Emission from the Nonirradiated Disk*

For a thin, nonirradiated accretion disk, the source of the disk blackbody emission is the viscous dissipation inside the disk. The dissipation rate D per unit area sets the effective temperature and flux from both surfaces of the disk,

$$D = \frac{9}{4}\nu\Sigma\Omega_{\rm K}^2 = 2\sigma T_{\rm eff}^4. \quad (1)$$

The surface density and the corresponding dissipation rate profile at a given time are obtained by numerically solving the diffusion equation (see Ertan & Alpar 2003 for details). The effective temperatures are calculated for each radial grid point. We obtain the model IR luminosity by integrating the blackbody fluxes along the spatial grid points emitting in the observational IR

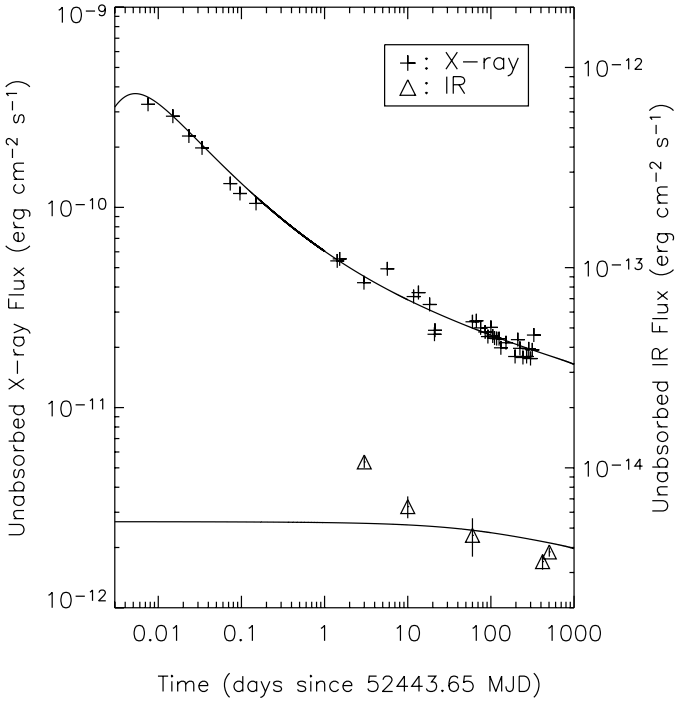

FIG. 1.—X-ray (*plus signs*) and IR (*triangles*) energy flux data of the enhancement phase of 1E 2259+586. The solid lines are the nonirradiated disk model curves.

band (K_s, $\lambda = 2.15\ \mu$m, width $= 0.31\ \mu$m). The blackbody temperature that mainly emits in this band is $kT_{\rm eff} \sim 0.2$ eV. For the model fits, we relate the model IR luminosities to the observed flux by $F_{\rm IR} \sim L_{\rm IR} \cos i/(4\pi d^2)$, where i is the inclination angle between the normal of the disk plane and the line of sight of the observer.

The model puts an upper limit to the fraction f of the disk mass flow rate that is accreted onto the neutron star. This upper limit is obtained by setting $\cos i = 1$. For the model given in Figure 1, $f = 0.03$ and $\cos i = 0.9$. The other model parameters are given in Table 1. It is seen in Figure 1 that the nonirradiated disk model is consistent with the long-term evolution of the IR data (∼1.5 yr), but not for the first two weeks.

2.3. *Infrared Emission from the Irradiated Disk*

A likely reason for this discrepancy is the irradiation of the disk by the X-rays from the neutron star. For a disk irradiated by the X-rays from the neutron star, the irradiation flux through the disk surface must be added to the dissipative energy flux in equation (1). The X-ray irradiation flux can be written as

$$F_{\rm irr} = \sigma T_{\rm irr}^4 = C\frac{\dot{M}_{\rm in}c^2}{4\pi R^2}, \tag{2}$$

where (Shakura & Sunyaev 1973)

$$C = \eta(1-\epsilon)\frac{H_{\rm irr}}{R}\left(\frac{d\ln H_{\rm irr}}{d\ln R} - 1\right), \tag{3}$$

η is the efficiency of the conversion of the rest mass energy into X-rays, ϵ is the X-ray albedo of the disk face, R is the radial coordinate, and $H_{\rm irr}$ is the pressure scale height of the disk, which should be calculated including the effect of the X-ray irradiation (Dubus et al. 1999). The disk thickness to radial distance ratio H/R is roughly constant along the disk. The parameter C can vary in a large interval, especially due to the uncertainty on the disk albedo ϵ. For a point irradiation source, estimates are usually in the range 10^{-4} to 10^{-3} (Tuchman et al. 1990; de Jong et al. 1996; Dubus et al. 1999). Using C as a free parameter, we calculate the effective temperature for the irradiated disk as

$$\sigma T_{\rm eff}^4 = \frac{D}{2} + F_{\rm irr}. \tag{4}$$

Equation (2) shows that $T_{\rm irr} \propto R^{-1/2}$, while $T_{\rm eff} \propto R^{-3/4}$ for a nonirradiated disk. For small radii viscous heating dominates over the X-ray heating. Beyond some critical radius R_c, depending on the irradiation strength, the main source of the emission from the disk surface is the reprocessed X-rays for an irradiated disk. The critical radius R_c can be estimated by equating the irradiation flux $F_{\rm irr}$ to the dissipative energy flux $D/2$ (eq. [1]). Assuming that the mass inflow rate at a given time is constant along the disk, we obtain

$$R_c = \frac{3}{2}\frac{GM_*}{Cc^2} \simeq f\left(\frac{10^{-4}}{C}\right)3\times10^9\ {\rm cm}. \tag{5}$$

We follow the same method as that for the nonirradiated disk model to calculate the total IR luminosity in the observational IR (K_s) band. In the vertical disk analyses, the X-rays are usually

TABLE 1

MODEL PARAMETERS FOR THE FLUX EVOLUTION PRESENTED IN FIGURES 1 AND 2

PARAMETER	NONIRRADIATED DISK MODEL	IRRADIATED DISK MODEL	
		Surface Density 1	Surface Density 2
$\Sigma_{\rm max}$ (g cm^{-2})	7.5×10^2	1.5×10^2	3.5×10^2
Gaussian width (cm)	2.0×10^7	2.0×10^7	1.1×10^7
$\Sigma_0/\Sigma_{\rm max}$	0.6	0.6	0.3
R_0 (cm)	1.0×10^9	1.0×10^9	1.0×10^9
$R_{\rm in}$ (cm)	8.3×10^8	8.5×10^8	8.5×10^8
p	0.7	0.65	0.65
f	0.03	0.27	0.27
$\cos i$	0.9	0.76	0.76

NOTES.—The three model curves in Fig. 3 have the same parameters as given in the first column of the irradiated disk model, but for different p values (0.60, 0.65, and 0.70). See § 3 for the explanation of the parameters here.

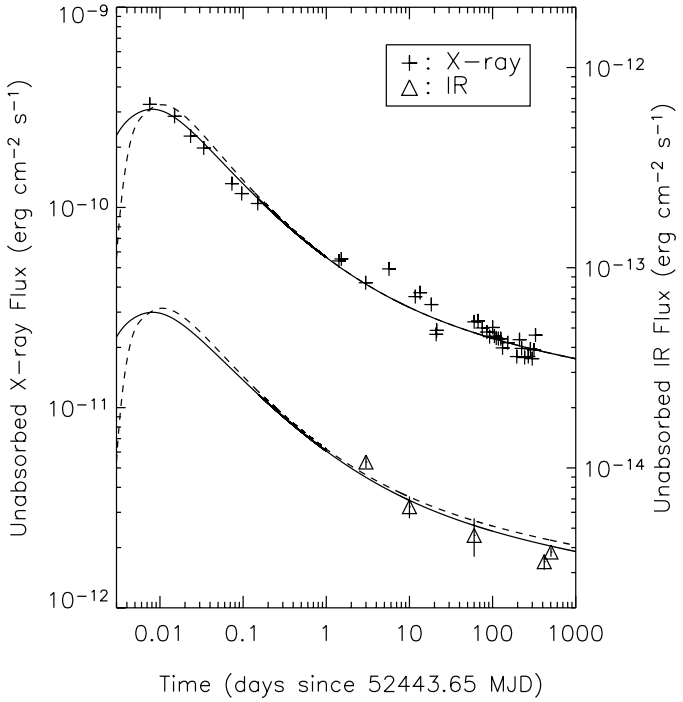

FIG. 2.—X-ray (*plus signs*) and IR (*triangles*) energy flux data of the enhancement phase of 1E 2259+586 and irradiated disk model curves. Dashed and solid curves are for two different initial Gaussian surface density distributions (see Table 1 for the model parameters).

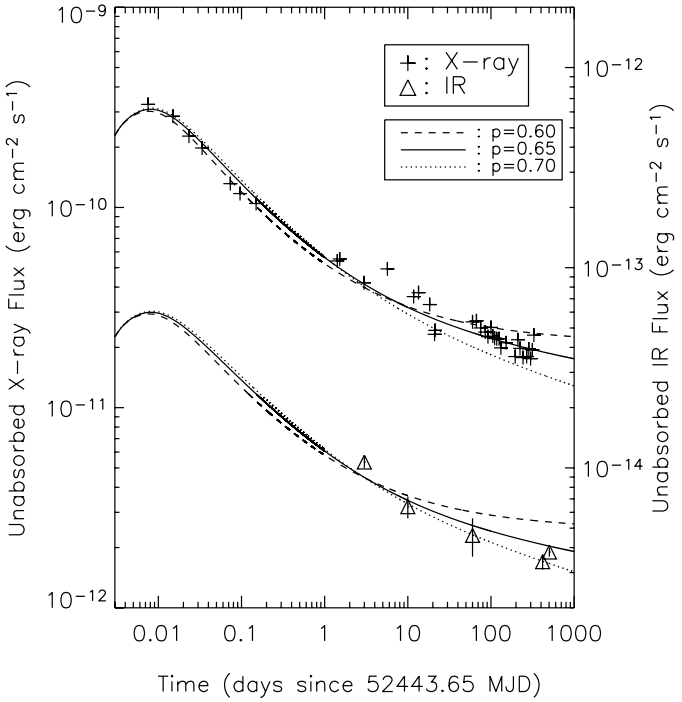

FIG. 3.—X-ray (*plus signs*) and IR (*triangles*) energy flux data of the enhancement phase of 1E 2259+586. The irradiated model curves correspond to different power-law indices p of the initial extended outer disk surface density distribution. The other disk parameters are the same for all three curves.

assumed to be absorbed in a thin layer of the disk surface. The irradiation modifies the vertical temperature profile and the effective temperature of the disk without significantly affecting the disk midplane temperatures that determine the kinematic viscosity (Dubus et al. 2001). Therefore, X-ray irradiation does not change the evolution of the disk mass transfer rates as long as the disk remains at the same viscosity state (see § 3). The irradiated disk model cannot constrain the f parameter, since there is the extra free parameter C. The model X-ray and IR flux curves given in Figures 2 and 3 were obtained with $C = 2 \times 10^{-4}$ and $f = 0.26$ for $\cos i = 0.76$. When we take f near unity with $\cos i = 0.76$, a similar model fit is obtained with $C \simeq 5 \times 10^{-5}$. The annular disk section radiating in the K_s band is at a radial distance $R \sim 2 \times 10^{11}$ cm at the beginning of the enhancement and shrinks slowly to $R \sim 5 \times 10^{10}$ cm along the decay phase, remaining in the irradiation-dominated part of the disk. Figures 2 and 3 show that this particular irradiated disk model is in agreement with both the X-ray and the IR data.

3. RESULTS AND DISCUSSION

The model X-ray and IR light curves are presented for the nonirradiated (Fig. 1) and irradiated (Figs. 2 and 3) disk models. The corresponding model parameters are given in Table 1. The differences between the initial surface density distributions of the best-fitting models are their amplitudes and a small change in the power-law index p of the extended disk profiles. In the irradiated disk model, since the effective temperatures are mainly determined by the irradiation flux rather than the viscous flux, the amplitude of the initial surface density distribution is less than that of the nonirradiated disk model (by a factor of $\sim$5). The time evolution of the mass accretion rate $\dot{M}$ onto the neutron star, which is observed as the X-ray light curve, is similar for all different models of the disk. For a given initial mass distribution, the evolution of the mass flow rate $\dot{M}$ through the disk is the same for both models, as the irradiation has no significant effect on the disk midplane temperatures. In the hydrogen disk models employed to account for the observed outbursts of dwarf novae and soft X-ray transients, the disk has two states. The viscosity parameter α is large (small) when the effective temperature of the disk is high (low) compared to a critical temperature reflecting the ionization of hydrogen ($\sim 10^4$ K). A local disk instability can lead to an outburst (quiescence) if the resulting heating (cooling) wave can take all or most of the disk to the high (low) viscosity state. The inclusion of the X-ray irradiation in models modifies significantly the critical accretion rates at which these instabilities occur. Nevertheless, for a given stable state, the effect of irradiation on disk mass flow evolution is small. The critical mass flow rates and the critical temperatures for disk instabilities depend on the exact composition of the disk material, which determines the opacities in the disk (Menou et al. 2002). Menou et al. use a carbon-oxygen composition to discuss disk instabilities. This composition is uncertain for AXP and SGR disks. In all our calculations, we use the electron-scattering opacity, as we previously did for SGR 1900+14. During our simulations we kept the viscosity parameter constant at the value $\alpha = 0.08$, which is characteristic of the hot states in hydrogen disk models. We also tested disk models with both high and low viscosity states (bimodal) going through the hydrogen ionization temperature. We used α-parameters similar to those of hydrogen disk models ($\alpha_{\rm hot} \sim 0.1$ and $\alpha_{\rm cold} \sim 0.01-0.05$). For a critical effective temperature $\sim 10^4$ K, both X-ray and IR model curves deviate from the observed trend of the light curves significantly, following the instability. The X-ray enhancement light curve of the SGR 1900+14 can also be reproduced by using a constant α-parameter $\alpha \sim 0.1$ (Ertan & Alpar 2003). Secular decay of the light curves implies that in the accretion regime indicated by the observed X-ray luminosities of the AXPs and SGRs, fallback disks do not experience a global disk instability.

The rise and early decay phases (the first few days of enhancement) of the X-ray luminosity are determined by the release of the Gaussian surface density distribution, representing the postburst pileup. In this phase, X-ray model curve evolution depends mainly on the amount of mass included in the Gaussian and the distance between the Gaussian center (R_0) and the disk's inner radius, rather than the detailed Gaussian parameters. The two model light curves seen in Figure 2 are for two different initial Gaussian surface density distributions with the same extended (outer) disk profile. The constant inner disk radius $R_{\rm in}$ was taken near the Alfvén radius for a dipole magnetic field with a strength of $\sim 10^{12}$ G on the stellar surface and $\dot{M}_{\rm in} \sim 10^{15}$ g s^{-1}. Similar fits can also be obtained for larger $R_{\rm in}$ and R_0. The model fits do not constrain the dipole magnetic field strength. For the first few weeks, the decay phase does not strongly depend on the chosen power-law index p of the extended model disk surface density profile, provided that it remains roughly around its best-fit value for the overall evolution curve. About a few weeks after the onset of the enhancement, light-curve evolution becomes sensitive to the power index p. For a steady disk, p is expected to be around 3/4, taking the run of the midplane temperatures as $R^{-3/4}$. This value of p is close to our best-fit p-parameters for both irradiated and nonirradiated disk models (0.65 and 0.70). In Figure 3 we illustrate three irradiated disk model light curves for different p-values (0.60, 0.65, and 0.70), keeping the Gaussian parameters constant. Irradiated and nonirradiated models are successful in explaining the long-term X-ray enhancement data. The nonirradiated disk model can reproduce the IR data except for the first two weeks with a low upper limit $f \leq 0.03$ for the accretion rate to disk mass flow rate ratio f. The irradiated disk model gives a better fit to the overall IR data without constraining f, due to the uncertainty in the efficiency of the X-ray irradiation for the AXP and SGR disks, which is likely to be different from that for low-mass X-ray binary (LMXB) disks. For LMXBs the optical to X-ray luminosity ratios are much higher than the ratio of the expected optical luminosity from the intrinsic dissipation of the disk and the X-ray luminosity from the neutron star surface. While this indicates that the optical fluxes of LMXBs are from an X-ray-irradiated disk, theoretical calculations of the disk thickness profile show that irradiation must be indirect because of the self-screening of the disk (see, e.g., Dubus et al. 1999). The most likely source of the indirect emission is a hot scattering corona above and below the central disk region. The hot corona can be fed by the thermally unstable, optically thin surface layers of the hot innermost disk. Is it plausible that the SGR and AXP disks have the same X-ray irradiation efficiency as that of LMXBs? This is not likely, because the stronger magnetic fields of SGRs and AXPs cut the disk at radii 2–3 orders of magnitude larger than the inner disk radii of LMXBs. For the irradiated disk model, we initially fix the parameter $f = \dot{M}_*/\dot{M}_{\rm in}$ and try to obtain a good fit to the X-ray data points first. Then, we look for the best fit to the IR light curve tracing the irradiation strength C. The irradiated disk model curves presented in Figures 2 and 3 are obtained with $f \simeq 1/4$, $\cos i \simeq 3/4$, and $C = 2\times 10^{-4}$. We see that fits with similar quality can be obtained for $fC\cos i \sim 4\times 10^{-5}$.

The gamma-ray burst energy required to build up the initial conditions of our models can be estimated by assuming that the postburst pileup represented by a Gaussian surface density distribution was accumulated near the inner disk radius just before the burst. The mass δM of the Gaussian distributions is $\sim 8\times 10^{20}$ and $\sim 1.6\times 10^{20}$ g for the nonirradiated and irradiated models, respectively. The amount of energy needed to push these masses from the inner disk radius $R_{\rm in}$ to R_0 obtained from the best model fits are 2.6×10^{37} and 5.2×10^{36} ergs. For an isotropic burst, the fraction of the burst energy absorbed by the disk is $2\pi R(2h)/(4\pi R^2) = h/R$, which is nearly constant along the disk and about a few $\times 10^{-3}$ for the accretion regime of the AXP 1E 2259+586. Then, the required total burst energies are about 10^{40} ergs for the nonirradiated disk model and 2×10^{39} ergs for the irradiated disk model. If the burst took place before the *RXTE* observations presented here, a burst duration of more than about 20 s for the nonirradiated disk is enough for the burst luminosity to remain under the detection limit of the *Ulysses* gamma-ray detectors that were active before the *RXTE* observations (Woods et al. 2004). For the burst energy expected from the irradiated disk model, the burst duration must be longer than only $\sim$5 s for the burst not to be detectable by the *Ulysses* gamma-ray detectors.

4. CONCLUSION

We have shown by means of numerical fits to data that the long-term ($\sim$1.5 yr) contemporaneous X-ray and IR energy flux data of the AXP 1E 2259+586 can be accounted for by the evolution of the disk after inner disk matter is initially pushed back by a burst. The estimated burst energy from the initial conditions of both irradiated and nonirradiated disk models is small enough to remain below the detection limits of the *Ulysses* gamma-ray detectors operating before the enhanced X-ray observations.

Both irradiated and nonirradiated disk models can reproduce the X-ray enhancement data. The irradiated disk model is also in agreement with the overall IR light curve accompanying the X-ray enhancement. The nonirradiated disk model gives a slower decay than that indicated by the first two IR data points, corresponding to about 3 and 10 days after the onset of the X-ray enhancement. Nevertheless, it is consistent with the subsequent 1.5 yr long-term IR data. Since the early decay phase could depend on the details of the initial disk conditions, we cannot exclude the nonirradiated disk model.

It is not possible to compare the active and passive disk models on the basis of the IR (K band) data (for a given X-ray light curve). Since the emission in this band comes from the irradiation-dominated outer part of the disk, the same IR radiation would be expected to be observed in either model. However, expectations of the two models are different for the shorter wavelength optical emission (R, V, and B bands) and their relation to the X-ray flux. For an active disk with a mass inflow rate of $\sim 10^{14}$–10^{15} g s^{-1}, a significant fraction of the emission in these optical bands comes from the intrinsic dissipation near the innermost disk radius. Dissipation gives rise to certain amount of mass inflow and thereby to accretion, since this mass inflow is near the corotation radius for relevant mass inflow rates. Our model thus expects a correlation also between the dissipation-dominated optical (R, V, and B bands) luminosity and the X-ray luminosity. (Note that an inner disk emitting in the optical indicates that the dipole magnetic field is $\sim 10^{12}$ G for relevant disk mass inflow rates.) Furthermore, any characteristic variation in the dissipation-dominated part of the optical luminosity is expected to be followed in X-rays with a delay characterized by the viscous timescale of the inner disk (hours to days in persistent states, and much shorter in the early enhancement phase due to large pressure gradients). For AXPs, in the persistent phase our model can estimate the dissipation-dominated optical flux using X-ray, IR, and interstellar extinction information, which requires a detailed source-by-source examination of the AXPs (work in progress). For AXP 1E 2259+586, we estimate that the luminosities in the K_s and R bands are nearly the same, and their ratios to the X-ray luminosity are about 10^{-4} in its persistent

state. At present, we cannot use this point to distinguish between our model and passive disk models like that of Rea et al. (2004), because only upper limits exist for the *R*- and *V*-band luminosity of AXP 2259+586. However, this remains as a distinguishing prediction of our model.

We acknowledge support from the Astrophysics and Space Forum at Sabancı University. M. A. A. acknowledges partial support from the Turkish Academy of Sciences. E. G. acknowledges support from the Turkish Academy of Sciences through a grant EG/TÜBA-GEBİP/2004-11.

REFERENCES

Alpar, M. A. 2001, ApJ, 554, 1245
Chatterjee, P., Hernquist, L., & Narayan, R. 2000, ApJ, 534, 373
Colpi, M., Geppert, U., & Page, D. 2000, ApJ, 529, L29
de Jong, J. A., van Paradijs, J., & Augusteijn, T. 1996, A&A, 314, 484
Dhillon, V. S., et al. 2005, MNRAS, 363, 609
Dubus, G., Hameury, J.-M., & Lasota, J.-P. 2001, A&A, 373, 251
Dubus, G., Lasota, J.-P., Hameury, J.-M., & Charles, P. 1999, MNRAS, 303, 139
Duncan, R. C., & Thompson, C. 1992, ApJ, 392, L9
Ekşi, K. Y., & Alpar, M. A. 2003, ApJ, 599, 450
Ertan, Ü., & Alpar, M. A. 2003, ApJ, 593, L93
Ertan, Ü., & Cheng, K. S. 2004a, ApJ, 605, 840
———. 2004b, NewA, 9, 503
Feroci, M., Hurley, K., Duncan, R., & Thompson, C. 2001, ApJ, 549, 1021
Hulleman, F., Tennant, A. F., van Kerkwijik, M. H., Kulkarni, S. R., Kouveliotou, C., & Patel, S. K. 2001, ApJ, 563, L49
Hulleman, F., van Kerkwijik, M. H., & Kulkarni, S. R. 2000, Nature, 408, 689
———. 2004, A&A, 416, 1037
Hurley, K. 2000, in AIP Conf. Proc. 526, Gamma-Ray Bursts: Fifth Huntsville Symp., ed. R. M. Kippen, R. S. Mallozzi, & G. J. Fishman (New York: AIP), 763
Hurley, K., et al. 1999, Nature, 397, 41
Israel, G. L., et al. 2002, ApJ, 580, L143
———. 2003, ApJ, 589, L93
———. 2004, ApJ, 603, L97
Kaspi, V. M., et al. 2003, ApJ, 588, L93
Kern, B., & Martin, C. 2002, Nature, 417, 527
Marsden, D., Lingelfelter, R. E., Rothschild, R. E., & Higdon, J. C. 2001, ApJ, 550, 397
Mazets, E. P., Cline, T., Aptekar, R. L., Butterworth, P., Frederiks, D. D., Golenetskii, S. V., Il'inskii, V. N., & Pal'shin, V. D. 1999, Astron. Lett., 25, 635
Mazets, E. P., Golenetskii, S. V., Il'inskii, V. N., Aptekar, R. L., & Guryan, Y. A. 1979, Nature, 282, 587
Menou, K., Perna, R., & Hernquist, L. 2002, ApJ, 564, L81
Mereghetti, S., Chiarlone, L., Israel, G. L., & Stella, L. 2002, in Proc. 270th WE-Heraus Seminar on Neutron Stars, Pulsars, and Supernova Remnants, ed. W. Becker, H. Lecsch, & J. Trümper (MPE Rep. 278; Garching: MPE), 29
Palmer, D. M., et al. 2005, Nature, 434, 1107
Rea, N., et al. 2004, A&A, 425, L5
Shakura, N. I., & Sunyaev, R. A. 1973, A&A, 24, 337
Tam, C. R., Kaspi, V. M., van Kerkwijk, M. H., & Durant, M. 2004, ApJ, 617, L53
Thompson, C., & Duncan, R. C. 1995, MNRAS, 275, 255
———. 1996, ApJ, 473, 322
Tuchman, Y., Mineshige, S., & Wheeler, J. C. 1990, ApJ, 359, 164
Wang, Z., & Chakrabarty, D. 2002, ApJ, 579, L33
Woods, P. M., Kouveliotou, C., Göğüş, E., Finger, M. H., Swank, J., Smith, D. A., Hurly, K., & Thompson, C. 2001, ApJ, 552, 748
Woods, P. M., et al. 2004, ApJ, 605, 378